Propagation of light beams in anisotropic nonlinear media: From symmetry breaking to spatial turbulence

A. V. Mamaev* and M. Saffman
Department of Optics and Fluid Dynamics, Risø National Laboratory, Postbox 49, DK-4000 Roskilde, Denmark

D. Z. Anderson and A. A. Zozulya
JILA, University of Colorado, C.B. 440, Boulder, Colorado 80309-0440
(Received 13 December 1995)

We investigate theoretically and experimentally breakup and subsequent spatial dynamics of (1+1)- and (2+1)-dimensional beams in bulk media with an anisotropic photorefractive nonlinear response. [S1050-2947(96)02207-X]

PACS number(s): 42.65.Jx, 42.65.Tg, 42.65.Hw

I. INTRODUCTION

Propagation and spatial evolution of light beams in nonlinear media is a central topic of nonlinear optical dynamics. There has been continuing interest in this topic since the initial investigations of self-trapping of light beams in nonlinear media [1,2]. Analysis of the stability and nonlinear evolution of solitary-wave solutions of nonlinear propagation equations is one of the most crucial parts of the problem of self-trapping of optical beams. Exact (1+1)-dimensional solitary-wave solutions to the nonlinear Schrödinger equation were found more than 20 years ago [3,4]. It was shown shortly thereafter [5] that these solutions are unstable in the case of a (1+1)-dimensional stripe solitary-wave propagating in a (2+1)-dimensional bulk nonlinear medium. The symmetry-breaking instability, which is due to the growth of perturbations along the initially homogeneous coordinate parallel to the stripe, is known as a transverse modulation instability and goes back to papers by Bespalov and Talanov [6] and Benjamin and Feir [7], who discussed its manifestations for a homogeneous (plane-wave) ground state. Although much theoretical work has been devoted to studying the instability of stripe solitary waves in both focusing and defocusing bulk media [8–12], the transverse modulation instability has only recently been observed experimentally [13–15].

Our topic here is a theoretical and experimental study of this instability in bulk photorefractive media with an anisotropic focusing or defocusing nonlinear response. Bright stripe solitary solutions in focusing media decay into a line of bright filaments, while dark stripe solitary solutions in defocusing media are subject to a snake instability [5] and decay into a line of optical vortices [10,11]. When the initial conditions are not solitary solutions the beam cannot propagate intact in the nonlinear medium. Wider stripe beams radiate and decay into multiple stripes before the onset of the instability seen for solitary stripes. For beams that are not too wide the stripes interact with each other and decay into a partially ordered pattern of filamentation. A related instability in planar photorefractive waveguides has also been observed [16]. Circular beams with full (2+1)-dimensional symmetry decay into a spatially disordered pattern [17]. Experiments with input speckle beams demonstrate the difference in the spatial statistics of the output field due to focusing or defocusing nonlinearities. We present results illustrating all stages of spatial evolution from symmetry breaking and decay of a solitary stripe to generation of a turbulent array of cylindrical filaments.

Photorefractive crystals turn out to be very convenient for experimental study of these instabilities. Several groups have demonstrated self-focusing and self-defocusing in photorefractive media [18–21]. A large steady-state nonlinear response can be obtained with low-power visible lasers. Furthermore, the magnitude and sign of the nonlinearity (focusing or defocusing) are easily controlled with an external voltage. The physics of light propagation in photorefractive media is considerably different than in Kerr media that are described by the nonlinear Schrödinger equation. The photorefractive nonlinearity is due to the action of a static electric field that is generated by the optical beam. The electric field is found by solving a particular form of Poisson's equation for the electrostatic potential ϕ, with a source charge distribution due to light-induced charge transport. The photorefractive nonlinearity is thus nonlocal. Given the electrostatic potential, the perturbation to the refractive index is $\delta n_{ij} \sim r_{ijk} \partial \phi / \partial x_k$, where r is the electro-optic tensor. The anisotropic nature of r results in a highly anisotropic nonlinear response. These differences result in some instability signatures that are not seen in Kerr media. In particular, the pronounced striped filamentation seen at intermediate stages of the nonlinear decay is unique to anisotropic media. Nonetheless, the transverse modulation instability and the final decay into bright and dark filaments are universal.

II. GENERAL EQUATIONS

We describe propagation of an optical beam $B(\vec{r})$ in a photorefractive medium in the presence of an externally applied electric field and/or photogalvanic nonlinearity by the set of equations [22,23]

* Permanent address: Institute for Problems in Mechanics, Russian Academy of Sciences, Prospekt Vernadskogo 101, Moscow, 117526 Russia.

$$\left[\frac{\partial}{\partial x}-\frac{i}{2}\nabla^2\right]B(\vec{r})=is\frac{\partial\varphi}{\partial z}B(\vec{r}), \tag{1a}$$

$$\nabla^2\varphi+\nabla\ln(1+|B|^2)\nabla\varphi=\frac{\partial}{\partial z}\ln(1+|B|^2), \tag{1b}$$

where φ is the normalized electrostatic potential induced by the beam. The boundary conditions for the potential φ are $\nabla\varphi(\vec{r}\to\infty)\to 0$. The differential operator $\nabla=\hat{y}\partial/\partial y+\hat{z}\partial/\partial z$ acts on coordinates y and z perpendicular to the direction of propagation of the beam x. Equations (1) imply that the beam is propagating along one of the crystallographic axes and that one component of the electro-optic tensor is considerably larger than the rest. These assumptions correspond to our experimental geometry and choice of strontium barium niobate (SBN) as a photorefractive nonlinear medium. The dimensionless coordinates (x,y,z) are related to the physical coordinates (x',y',z') by the expressions $x=|\alpha|x'$ and $(y,z)=\sqrt{k|\alpha|}(y',z')$, where $\alpha=(1/2)kn^2r_{33}(E_{\rm ext}+E_{\rm ph})$. Here k is the wave number of electromagnetic radiation in the medium, $E_{\rm ph}$ is the amplitude of the photogalvanic field, and $E_{\rm ext}$ is the amplitude of the external field far from the beam. Both $E_{\rm ext}$ and $E_{\rm ph}$ are directed along the z coordinate. The electromagnetic intensity $|B(\vec{r})|^2$ is normalized to the dark intensity I_d. Positive values of the coupling parameter α correspond to self-focusing and negative to self-defocusing media, $s=\mathrm{sgn}\alpha=\pm 1$. The transformation from normalized to physical coordinates implies that the width of the solitary solutions given below scale as the square root of the electric field directed along the z coordinate.

Besides the Kerr-type part of the material response accounted for by Eqs. (1), the photorefractive nonlinearity also has an additive part of the response, due to diffusive charge transport, that results in asymmetric stimulated scattering (fanning) [24] and in the bending of the beam toward the $\hat{c}$ axis of the crystal [25,26]. This part is responsible for the photorefractive nonlinearity when both the applied electric field and the photogalvanic contribution are equal to zero. For typical nonlinear interactions and spatial structures of the electromagnetic field formed in photorefractive media in this case see Ref. [27]. The influence of the fanning terms on the photorefractive self-focusing has been analyzed in [22,23]. In the present paper we are interested in self-focusing and self-defocusing properties of photorefractive nonlinearity and the terms responsible for fanning have been removed from Eqs. (1).

If all functions in the system of equations (1) are assumed to depend only on the transverse coordinate z, Eq. (1b) can be integrated to yield

$$\frac{\partial\varphi}{\partial z}=\frac{|B|^2-|B_\infty|^2}{1+|B|^2}, \tag{2}$$

where $|B_\infty|=|B(z=\infty)|=|B(z=-\infty)|$. Using Eq. (2) the parabolic equation (1a) for the electromagnetic field can be recast in a form identical to that for a saturable Kerr nonlinearity

$$\left[\frac{\partial}{\partial x}-\frac{i}{2}\frac{\partial^2}{\partial z^2}\right]B(x,z)=is\frac{|B|^2-|B_\infty|^2}{1+|B|^2}B. \tag{3}$$

Stripe solitary-wave solutions of Eq. (3) for which the diffraction is compensated for by the nonlinearity are of the form $B(x,z)=b(z)\exp(i\Gamma_0 x)$, where Γ_0 is a real propagation constant. The simplest of these solutions in the focusing case $s=1$ is a symmetric localized bright beam with zero field at infinity $B_\infty=0$ and $\Gamma_0=1-b_m^{-2}\ln(1+b_m^2)$. Here $b_m=b(0)$ is the maximum value of the amplitude $b(z)$, governed by the relation [28]

$$(db/dz)^2=2[\ln(1+b^2)-(b^2/b_m^2)\ln(1+b_m^2)]. \tag{4}$$

The simplest stripe solitary-wave solution in the defocusing case $s=-1$ is an antisymmetric beam with finite intensity at infinity and a dark region of small intensity where the field passes through zero and changes sign. The propagation constant Γ_0 is in this case zero and the amplitude $b(z)$ is described by the relation [29]

$$(db/dz)^2=2\left[1+b^2-(1+b_m^2)-(1+b_m^2)\ln\frac{1+b^2}{1+b_m^2}\right], \tag{5}$$

where $b_m=b(\infty)=-b(-\infty)$.

Analysis of transverse modulation instability of the solitary-wave solutions (4) and (5) in the framework of Eqs. (1) has been reported in [30,13,14]. Sections III and V below deal with the analysis of the nonlinear stage of this instability for the focusing and defocusing cases, respectively.

To study spatial dynamics of (1+1)- and (2+1)-dimensional beams in photorefractive media Eqs. (1) have been solved numerically. The input electromagnetic field in the calculations was of the form

$$B(x=0,y,z)=B_0(y,z)[1+B_N(y,z)]\equiv B_0(y,z)+N(y,z), \tag{6}$$

where B_0 is a (1+1)- or (2+1)-dimensional ground state and B_N is an additive noise with uniform random spectrum in Fourier space along both y and z cooordinates. The noise has been specified by assigning uniformly distributed random complex numbers to all points on the computational grid and taking the inverse Fourier transform. The relative magnitude of noise is characterized by the parameter

$$\epsilon=\frac{\int|N(y,z)|^2dydz}{\int|B_0(y,z)|^2dydz}, \tag{7}$$

where the integration is carried out over the computation window $-l_y/2<y<l_y/2$, $-l_z/2<z<l_z/2$. Particular choices of the ground state B_0 are discussed below.

III. THEORY: FOCUSING CASE

The results of the nonlinear evolution of stripe (1+1)-dimensional beams can be conveniently visualized by subdividing the region of initial conditions into that covering narrow beams with characteristic widths of the order of the width of the solitary solution (4) and much wider beams. Narrow beams evolve in a fashion that is very similar to the solitary solution (4). They are structurally stable along the inhomogeneous coordinate z experiencing, at most, some radiative decay. Their breakup is due to the transverse modulation instability discussed in [30,13].

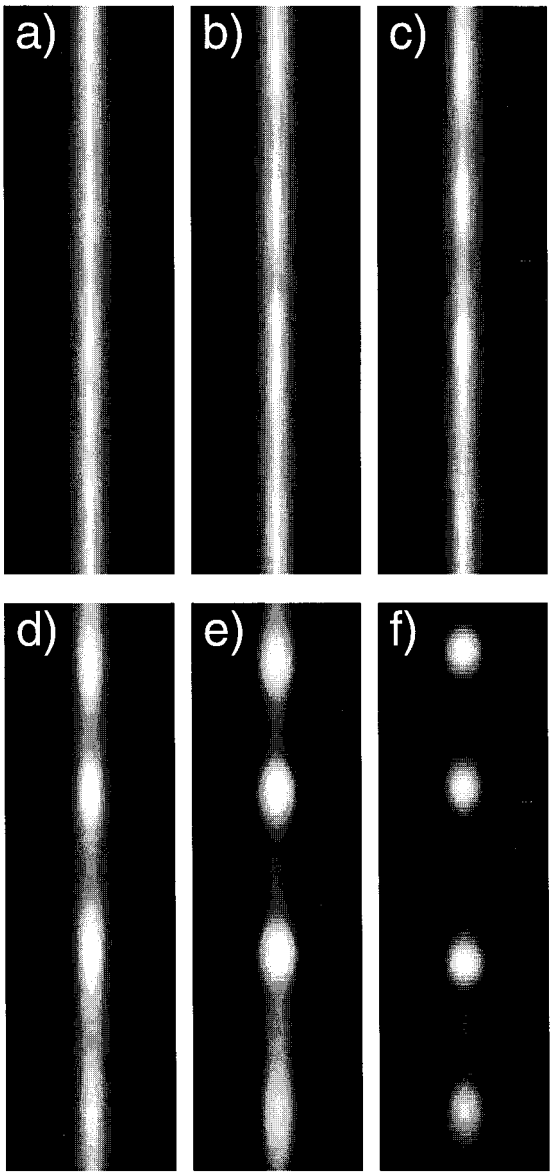

FIG. 1. Evolution of a narrow Gaussian stripe beam with $d=4.5$ and $I_m=3$ for propagation distances $x=5$ (a), 10 (b), 15 (c), 20 (d), 25 (e), and 30 (f). The z coordinate is horizontal and the y coordinate is vertical.

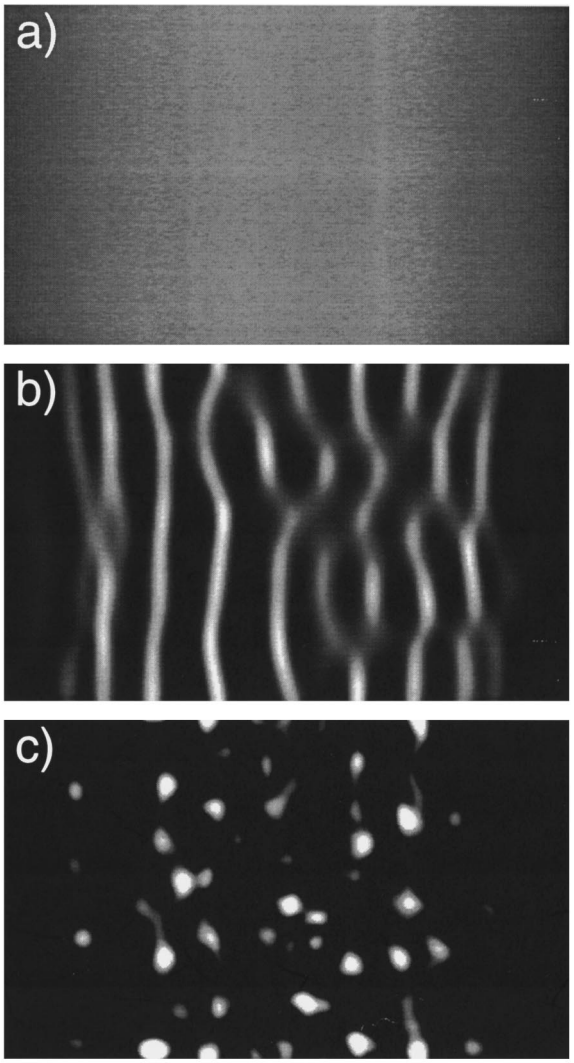

FIG. 2. Evolution of a wide super-Gaussian stripe beam with $d=4.5$ and $I_m=3$ for propagation distances $x=0$ (a), 15 (b), and 30 (c).

Figure 1 shows the results of the nonlinear evolution of a narrow stripe Gaussian beam $B_0(y,z)=\sqrt{I_m}\exp(-4z^2/d^2)$ with the initial diameter $d=4.5$, $I_m=3$, $l_y=60$, $l_z=20$, and $\epsilon=3\times10^{-2}$. The value of l_y that was used corresponds to about four periods of modulation for the fastest growing mode for $I_m=3$. Figure 1 shows the intensity distribution of the beam as it propagates in the nonlinear medium for a longitudinal propagation distance ranging from $x=5$ [Fig. 1(a)] to $x=30$ [Fig. 1(f)] in increments of 5. The initial diameter of the Gaussian beam was chosen to be close to that of a solitary solution (4), so the width of the beam remains roughly the same. For small propagation distances (small nonlinearities) the beam looks essentially unchanged, as seen in Figs. 1(a) and 1(b). At this initial stage of the breakup all spatial harmonics of the noise are small and each is amplified exponentially with its own growth rate. The fastest-growing modes become noticeable first [Fig. 1(c)] and at later stages determine the characteristic spatial scale of the breakup. At larger propagation distances (larger nonlinearities) the beam breaks up in a quasiperiodic series of $(2+1)$-dimensional filaments as shown in Figs. 1(d)–1(f).

In general there is no strict selection of a single transverse wave number and even at the nonlinear stage several of them (having large growth rates) are present with comparable amplitudes. As a result, the distance between adjacent filaments is not exactly the same and depends on the particular distribution of the noise, though the distance averaged over several filaments is in good correspondence to that determined by the fastest-growing modes of the transverse modulation instability. The intensities of different filaments are also different. Each of the filaments is ''breathing'' and changing its shape and amplitude with the longitudinal propagation distance. The peak intensities of the filaments oscillate between some maximum and minimum values in an apparently nonperiodic manner.

Results of numerical analysis of spatial evolution of a wide stripe beam are shown in Fig. 2. The initial conditions for this case correspond to the ground state being a super-Gaussian stripe $B_0(y,z)=\sqrt{I_m}\exp(-4z^4/d^4)$. The other pa-

rameters are $d=70$, $I_m=1$, $l_y=70$, $l_z=200$, and $\epsilon=3\times10^{-2}$. The values of the propagation distance x in Fig. 2 are equal to (a) 0, (b) 15, and (c) 30. The main distinguishing feature of Fig. 2 as compared to Fig. 1 is the loss of structural stability along the inhomogeneous coordinate z. The wide incident beam [Fig. 2(a)] first breaks down in a series of intertwined stripes [Fig. 2(b)] that subsequently evolve into a random pattern of (2+1)-dimensional filaments [Fig. 2(c)] in a manner similar to that for a narrow beam.

The initial breakup into stripes [Fig. 2(b)] is due to two reasons. First, even in the pure (1+1)-dimensional case when the homogeneous coordinate y is excluded from the analysis and the photorefractive nonlinearity is identical to a saturable Kerr nonlinearity, any wide stripe beam breaks down into narrower (1+1)-dimensional stripes. This phenomenon is analogous to the decay of an arbitrary initial condition into a set of solitons in the case of a (1+1)-dimensional nonlinear Schrödinger equation (a nonsaturable Kerr nonlinearity) and has been extensively investigated using the formalism of the inverse scattering method [31].

The second and more important reason for the initial breakup of a wide beam into stripes is due to the strongly anisotropic response of the photorefractive nonlinearity itself as is manifested by the structure of Eqs. (1). Even in the case of circularly symmetric initial conditions this anisotropy favors the decay along the coordinate z. It means that even initially circularly symmetric beams in photorefractive media will evolve in an anisotropic manner. To illustrate this point we have analyzed the spatial evolution of a wide initially circularly symmetric beam for the photorefractive nonlinearity given by Eqs. (1) and the isotropic saturable Kerr nonlinearity described by the equation

$$\left[\frac{\partial}{\partial x}-\frac{i}{2}\nabla^2\right]B(\vec{r})=i\frac{|B|^2}{1+|B|^2}B. \tag{8}$$

The initial condition for both cases corresponded to a Gaussian beam $B(y,z)=\sqrt{I_m}\exp(-4y^2/d^2-4z^2/d^2)$ with $d=100$ and $I_m=1$. The results of its evolution for the photorefractive and the Kerr nonlinearity are presented in Figs. 3 and 4, respectively. Despite its initial radial symmetry [Figs. 3(a) and 4(a)] the light beam in a photorefractive medium first breaks up into a series of intertwined stripes aligned along the y axis. Each of those subsequently decays into (2+1)-dimensional filaments in a manner similar to the breakup of a narrow stripe beam, resulting in the appearance of randomly located (2+1)-dimensional filaments. A radially symmetric beam in a saturable Kerr medium in the same conditions breaks up into a set of filaments without going through the stage of stripes since both the nonlinearity and the initial ground state are isotropic and there is no preferred direction for their formation. When the calculation is extended to longer propagation distances the array of filaments is observed to dance and breath in an apparently turbulent fashion.

IV. EXPERIMENT: FOCUSING CASE

The experimental arrangement was as described in Ref. [13]. A 10-mW beam from a He-Ne laser ($\lambda=0.6328\ \mu m$) was passed through a variable beam splitter and a system of

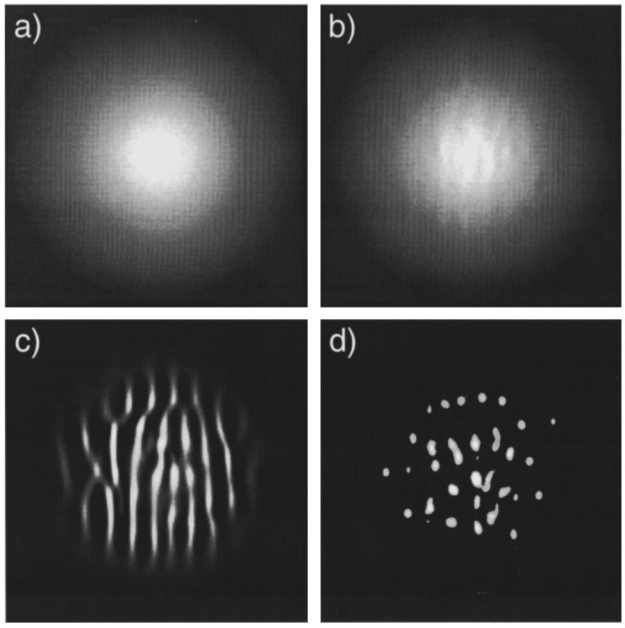

FIG. 3. Evolution of a radially symmetric Gaussian beam with $d=100$ and $I_m=1$ in a photorefractive medium for propagation distances $x=0$ (a), 5 (b), 15 (c), and 25 (d).

two cylindrical lenses controlling the size of the elliptical beam waist. The beam was directed into a photorefractive crystal of SBN:60 ($Sr_{0.6}Ba_{1-0.6}Nb_2O_6$), lightly doped with 0.002% by weight Ce. The beam propagated in the horizontal plane perpendicular to the crystal $\hat{c}$ axis and was polarized in the horizontal plane along the $\hat{c}$ axis to take advantage of the largest component of the electro-optic tensor of SBN. The crystal measured 10 mm along the direction of propagation and was 9 mm wide along the $\hat{c}$ axis. A variable dc voltage was applied along the $\hat{c}$ axis to control the value

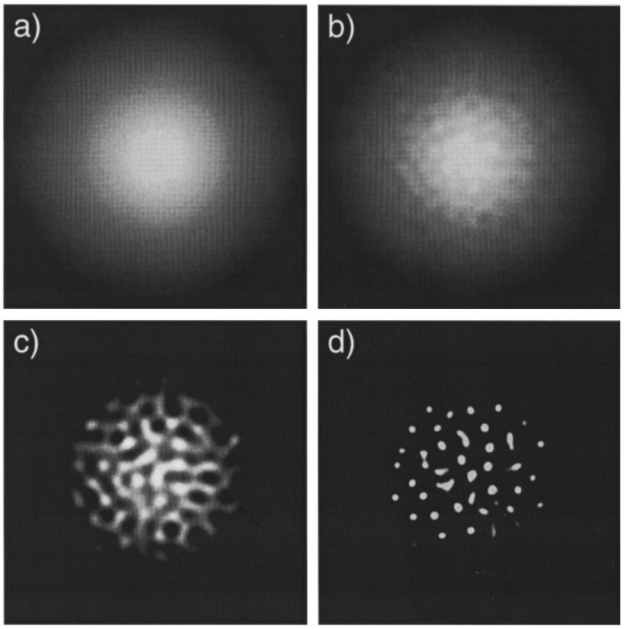

FIG. 4. Evolution of a radially symmetric Gaussian beam with $d=100$ and $I_m=1$ in a saturable Kerr medium for propagation distances $x=0$ (a), 5 (b), 10 (c), and 15 (d).

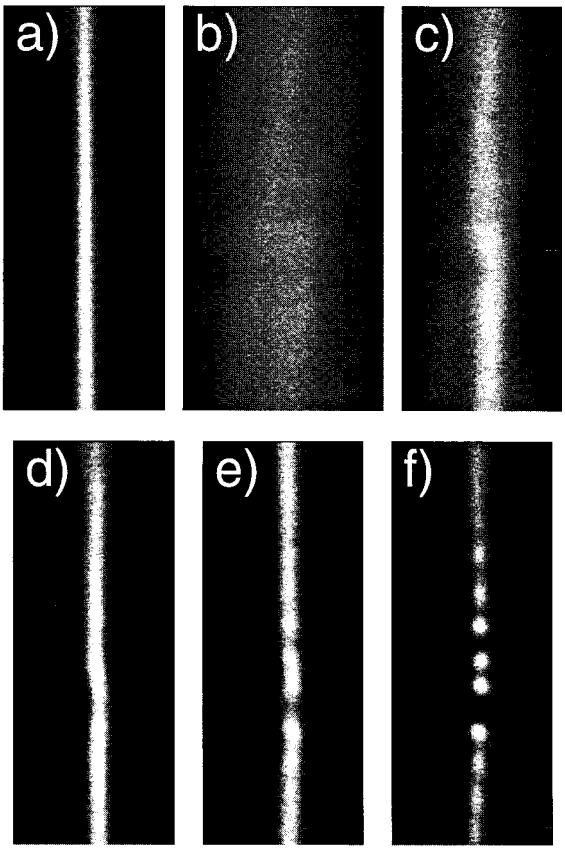

FIG. 5. Narrow bright stripe: (a) input (V=0) and (b)–(f) output near-field intensity distributions for applied voltage equal to 0 V (b), 620 V (c), 900 V (d), 1290 V (e), and 1790 V (f).

of nonlinear coupling and the effective dark intensity was varied by illuminating the crystal from above with incoherent white light. Images of the beam at the input and output faces of the crystal and of the far-field intensity distribution were recorded with a charge coupled device camera. All experimental results below were recorded under steady-state conditions. Experiments demonstrating planar self-focusing in bulk nonlinear media were initially reported some years ago [32], but the instability and spatial evolution of stripe beams demonstrated here and in [13] appear not to have been observed previously.

Figure 5 demonstrates the breakup of a narrow stripe beam (compare with the theoretical Fig. 1). In this experiment the elliptical beam waist measuring about 15 μm in the horizontal direction by 2 mm in the vertical direction was placed about 0.2 mm in front of the crystal so that the input beam in the crystal was diverging. Figure 5 shows the near-field distributions of the input [Fig. 5(a)] and the output [Figs. 5(b)–5(f)] beam for different values of the applied voltage (different values of the nonlinearity) and a fixed level of incoherent illumination several times weaker than the beam intensity. Figure 5(b) shows the diffractive spreading of the output beam for zero applied voltage (zero nonlinearity). As the nonlinearity increases the beam starts to self-focus [Fig. 5(c)] forming a self-trapped channel of light [Fig. 5(d)]. Increasing the nonlinearity unavoidably turns on the modulation instability. For larger nonlinearities the amplified noise grows to the extent of becoming noticeable [Fig. 5(e)] and the two-dimensional self-trapped beam breaks up into a

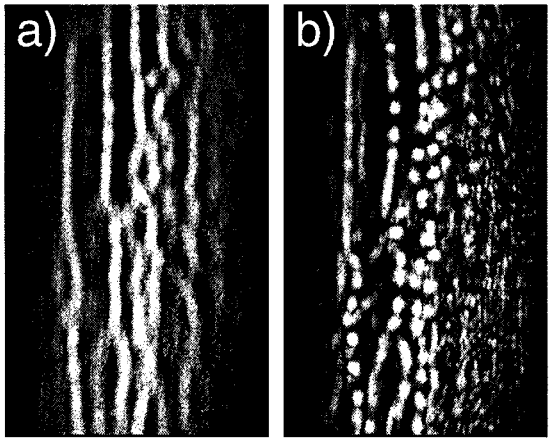

FIG. 6. Intermediate-width bright stripe: output near-field intensity distributions for applied voltage equal to (a) 1000 V and (b) 2000 V.

sequence of filaments [Fig. 5(f)]. No artificial seeding was added to the input beam. The instability developed from the natural level of noise present on the beam and/or in the crystal. Notice that of all possible harmonics the system chose those with the largest growth rates. The corresponding value of the wave number determines the spatial period of the modulation in Fig. 5(f). This period is equal to about 40 μm or $k_y/k \approx 0.015$ and is in agreement with the wave number of the fastest-growing modes obtained from the linear stability analysis of Ref. [30]. As the voltage was increased the center of the focused channel shown in Figs. 5(d)–5(f) was also displaced along the $\hat{c}$ axis by about two beam diameters due to photorefractive self-bending [25,26].

Increasing the diameter of the input beam several times resulted in the one-dimensional (along the z axis) self-focusing of this beam with its subsequent breakup into several narrower bright stripes, as shown in Fig. 6(a). For larger values of the applied voltage (larger values of the nonlinearity) each of these stripes in turn broke down into a series of bright spots due to the development of the transverse modulation instability [Fig. 6(b)] (compare with Fig. 2).

We have also studied the influence of the initial intensity distribution of the light on its subsequent self-focusing. Figure 7 demonstrates the evolution of a wide beam with an externally imposed regular intensity modulation. The initial distribution of the field was obtained by interfering two plane waves at a small angle. The initial intensity ratio of the waves equal to approximately 2.2:1 created a deep sinusoidal interference pattern at the entrance to the medium. The wave vector of the interference pattern coincided with the direction of the $\hat{c}$ axis. The stationary energy exchange between the two waves was insignificant due to the smallness of their crossing angle as compared to the characteristic Debye angle.

Figure 7(a) shows the output intensity distribution for zero applied voltage (zero nonlinearity). The spatial frequency of the interference fringes in Fig. 7(a) is equal to about 11 lines/mm. An increase in the voltage first resulted in self-focusing of each of those fringes [Fig. 7(b)], but for still larger voltages the fringes got somewhat broader. The same effect was observed previously in Ref. [33] using a photorefractive crystal of BSO (bismuth-silicon oxide). Presumably because the nonlinearity is much smaller in BSO

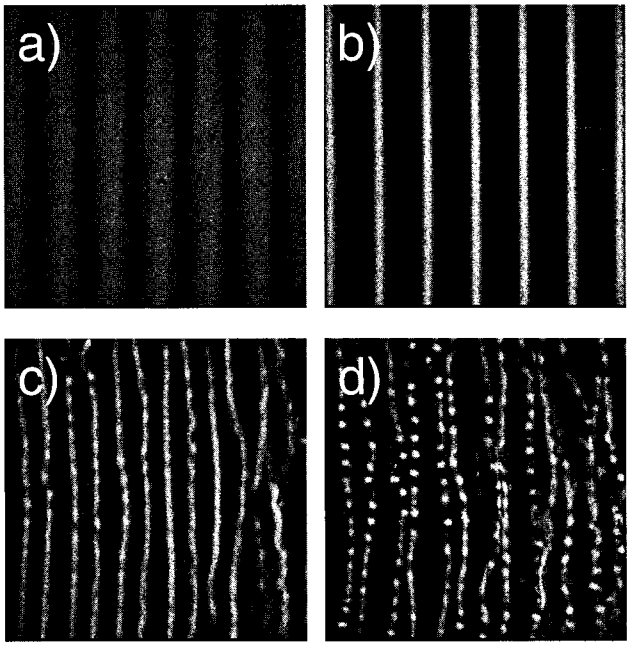

FIG. 7. Wide beam with externally imposed interference pattern: output near-field intensity distributions for applied voltage equal to (a) 0 V, (b) 450 V, (c) 1500 V, and (d) 2000 V.

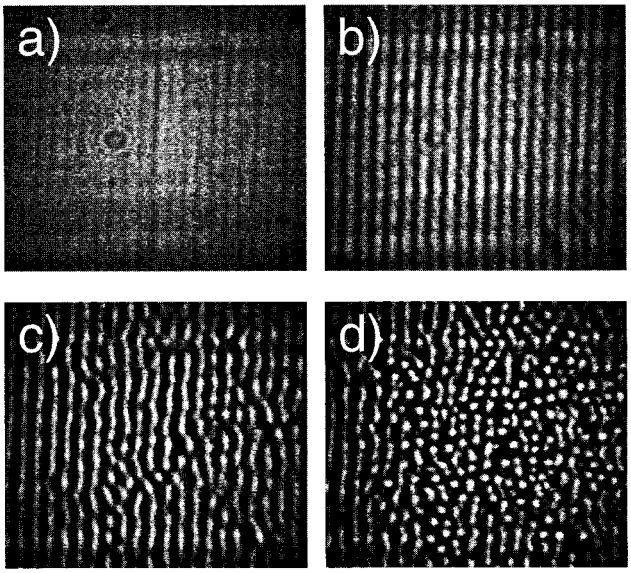

FIG. 8. Wide radially symmetric Gaussian beam: output near-field intensity distributions for (a) 0 V, (b) 600 V, (c) 1200 V, and (d) 1500 V, which show the central $0.8 \times 0.8\ \mathrm{mm}^2$ region of the beam.

than in the SBN used here, the subsequent spatial dynamics shown in Figs. 7(c) and 7(d) were not observed in Ref. [33]. A further increase in the voltage (the nonlinearity) resulted in the breakup of each of the fringes (bright stripes) into two fringes and their subsequent focusing [Fig. 7(c)]. At still larger values of the applied voltage the transverse modulation instability already visible in [Fig. 7(c)] broke up each of the bright stripes into a set of $(2+1)$-dimensional filaments [Fig. 7(d)]. The final number of bright stripes in Fig. 7(c) is twice that of the initial fringes in Fig. 7(a), demonstrating that the initial spatial scale in Fig. 7(a) is not optimum for the self-focusing. Similar experiments with the spatial frequency of the interference pattern about twice higher than in Fig. 7 resulted in a one-to-one correspondence between the initial and the final number of bright stripes.

The evolution of a wide initially radially symmetric beam (with characteristic diameter of about 1.5 mm) is shown in Fig. 8. The beam was, in this case, directed onto the crystal bypassing the system of cylindrical lenses. The registration system remained the same. Figure 8(a) shows the output intensity distribution in the central portion of the beam in the absence of applied voltage. A small horizontal modulation on the beam (less than 10%) is due to striations in the crystal. Increasing the value of the applied voltage resulted in self-focusing of each line. A further increase in the applied voltage resulted in increasing modulation depth of the lines. At larger values of the applied voltage each of the bright stripes breaks down into filaments following the same scenario as seen in Figs. 5–7. The final state (compare with Fig. 3) is a spatially disordered array of hundreds of bright filaments. It is worth noting that the filaments look approximately circular despite the anisotropy described by Eq. (1a). This is indicative of the global nature of Eq. (1b) for the potential.

V. THEORY: DEFOCUSING CASE

The dark stripe solitary solution (5) has infinite energy due to the nonzero value of the field at infinity. This creates obvious problems with experimental observations. Experimental studies of spatial dynamics of a dark stripe beam (intensity notch) in defocusing media have relied on embedding it in a wider bright beam [34,19,21]. Since the bright

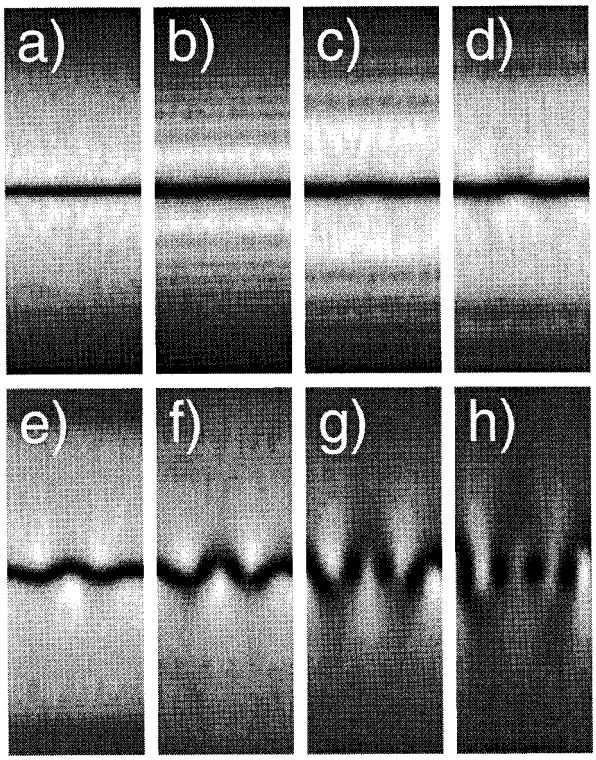

FIG. 9. Evolution of the dark stripe solitary solution (5) embedded in a wide Gaussian beam with diameter $d=100$ and $I_m=|b_\infty|^2=3$ for propagation distances from (a) $x=0$ to (h) $x=35$ changing in increments of five. The z coordinate is vertical and the y coordinate is horizontal.

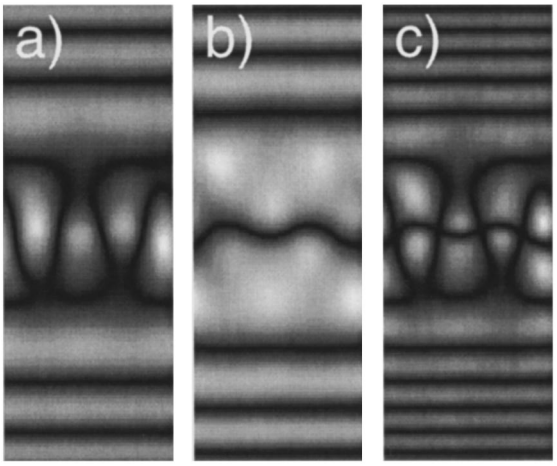

FIG. 10. (a) Real and (b) imaginary parts of the field for Fig. 9(h) and (c) their product.

envelope experiences defocusing, the background parameters for the dark stripe are continuously changing with the propagation distance. The intensity of the spreading bright beam can be kept at a high enough level only for a limited distance. Eventually, when it goes below the saturation intensity the nonlinearity essentially switches off. Furthermore, the bright beam has a finite transverse size. As a consequence of the above, the transverse instability growth rates calculated for, e.g., the solitary solution (5) embedded in a wider defocusing beam are somewhat lower than for the same solitary solution in its ''pure'' form. The qualitative physics of the breakup and the spatial dynamics remain essentially the same.

As in the case of focusing media it is convenient to separate the parameter region into that covering the evolution of narrow and wide striped beams. Typical results for evolution of a narrow dark striped beam are presented in Fig. 9. The ground state for this case has been chosen to have the form

$$B_0(z)=b(z)\exp(-4z^2/d^2), \tag{9}$$

where $b(z)$ is given by Eq. (5). The electromagnetic field (9) is the dark stripe solitary-wave solution (5) imbedded in a wide Gaussian beam with diameter d. Figure 9 demonstrates the spatial dynamics of the beam (9) with $d=100$, $I_m=|b(\pm\infty)|^2=3$, and $\epsilon=3\times10^{-2}$. As it propagates the

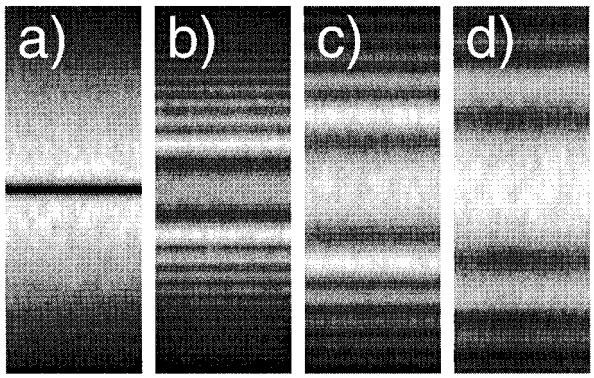

FIG. 11. Evolution of the dark stripe (10). All parameters are as in Fig. 9; $x=0$ (a), 5 (b), 10 (c), and 15 (d).

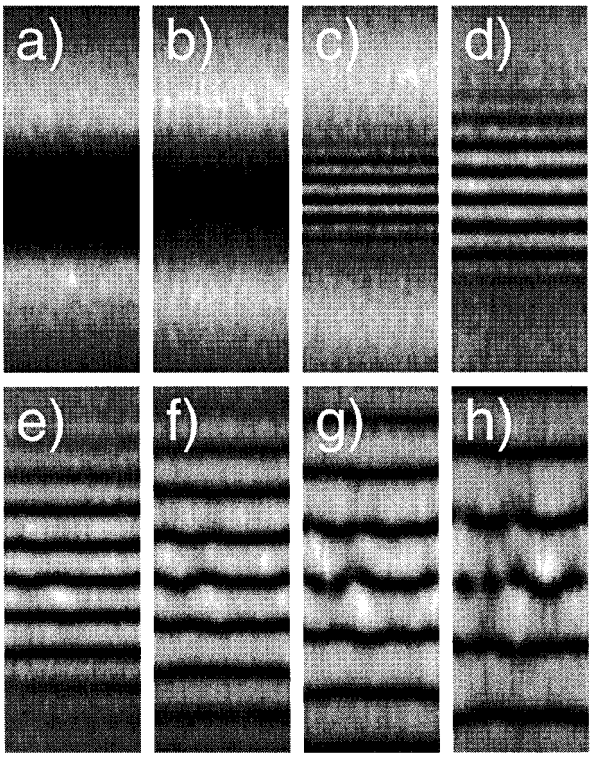

FIG. 12. Evolution of the wide dark stripe embedded in a Gaussian beam with $d=100$, $I_m=3$, and $\epsilon=3\times10^{-2}$. The propagation distance changes from (a) $x=0$ to (h) $x=35$.

wide bright envelope experiences self-defocusing. The dark stripe in the center first expands a bit [Figs. 9(b) and 9(c)], but otherwise remains unchanged. There is some small amount of radiative decay in Fig. 9(b)–9(f) with radiated waves seen as dark stripes on a brighter background that originate near the center of the beam and move outward. At larger propagation distances [Figs. 9(d) and 9(e)] the development of the snake instability results in the periodic bending of the dark channel along the initially homogeneous coordinate y. The dark line of zeros of the field breaks down

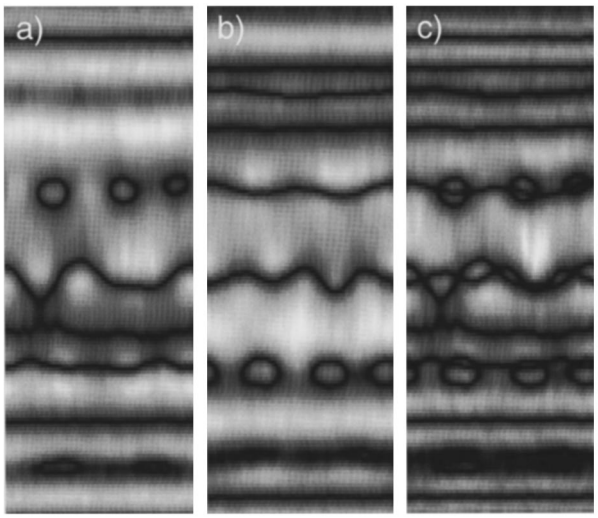

FIG. 13. (a) Real and (b) imaginary parts of the field for Fig. 12(h) and (c) their product.

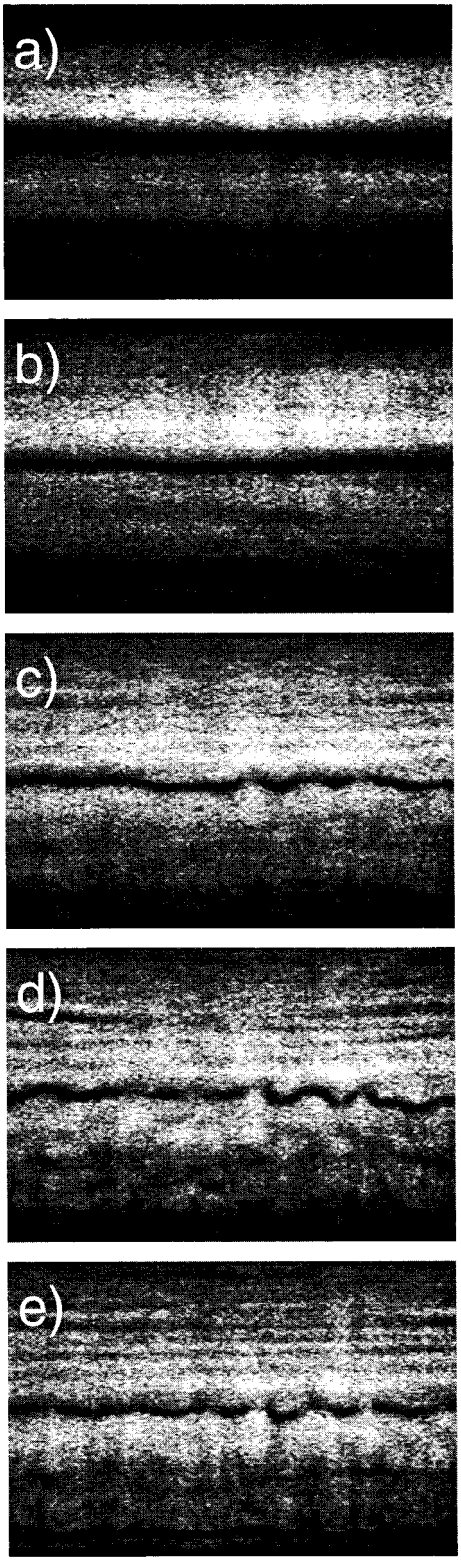

FIG. 14. Dark stripe: output near-field intensity distributions for applied voltages of (a) 0 V, (b) 620 V, (c) 900 V, (d) 1290 V, and (e) 1790 V.

into a set of optical vortices or wave-front dislocations that become more and more pronounced [Figs. 9(f)–9(h)].

These dislocations are shown in Fig. 10 by plotting the product of the real and the imaginary part of the electromagnetic field for the conditions of Fig. 9(h). Dark intertwined lines correspond to zeros of either the real or the imaginary part, the points of their intersection are zeros of the total field. Figure 10 shows the central part of the beam in Fig. 9 along the z coordinate.

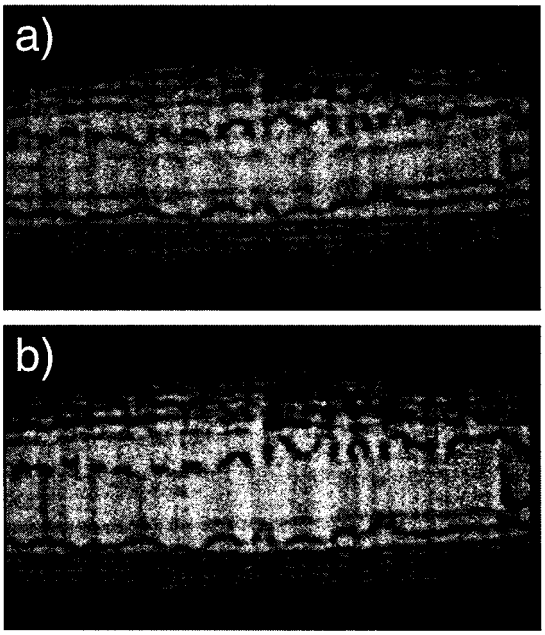

FIG. 15. Two dark stripes embedded in a bright beam: output near-field intensity distributions for (a) 1700 V and (b) 2000 V.

Figure 11 shows the spatial evolution of a dark stripe beam with the initial ground state given by the relation

$$B_0(z)=|b(z)|\exp(-4z^2/d^2). \tag{10}$$

The dark stripe beam (10) has the same intensity profile as the previously discussed beam (9). The only difference between them is that the field in Eq. (9) passes through zero and changes sign, whereas for Eq. (10) it just touches zero without acquiring an additional π phase shift. Spatial evolution of these fields is very different. Namely, the dark stripe beam (9) has a solitary-wave structure, whereas the beam (10) is very far from it. The dark stripe beam (10) cannot preserve its structural integrity along the coordinate z even when transverse effects due to the coordinate y are neglected. As seen in Fig. 11, the dark notch [Fig. 11(a)] decays into an intensity maximum surrounded by two minima, which in turn are surrounded by two intensity maxima when one goes from the center to the periphery of the beam. The intensity of the field does not reach zero even in the minima [Fig. 11(b)]. This scenario may be visualized as the decay of the intensity notch (5) into a pair of gray stripe beams [35] plus some amount of radiating waves that travel away from the center and spread out [Figs. 11(b) and 11(c)]. The initial stages of the evolution shown in Fig. 11 are in good agreement with the experimental observations of Ref. [19].

Figure 12 shows results of the spatial evolution of a wide stripe beam. The input distribution of the field is given by the equation

$$B_0(z)=\sqrt{I_m}\exp[-4z^2/d^2+i\pi\theta(z)]\Phi(z), \tag{11}$$

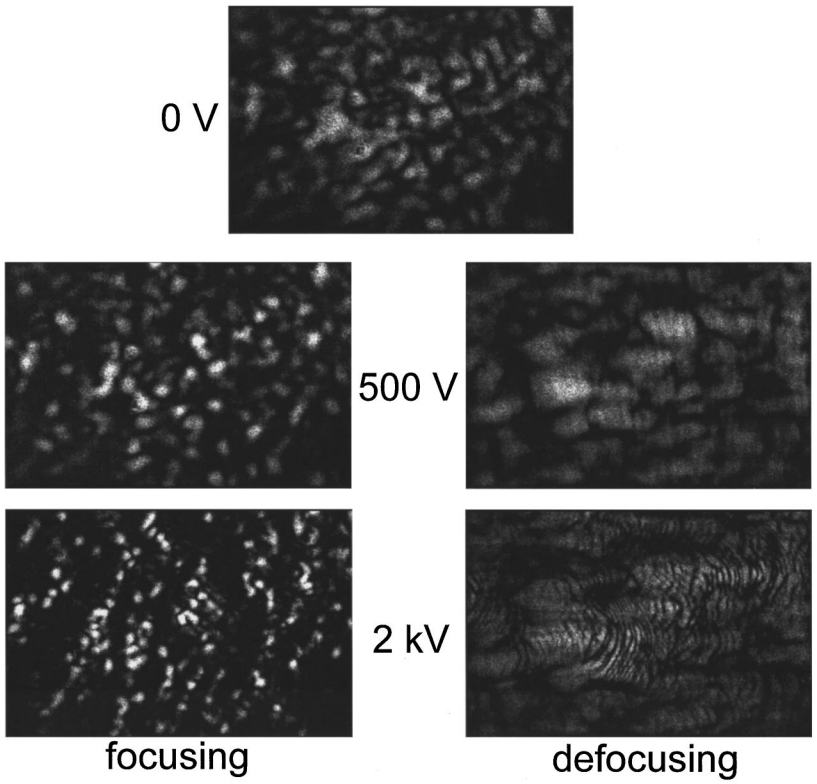

FIG. 16. Propagation of a speckle beam for focusing and defocusing nonlinearities. The top figure shows the output near field for zero nonlinearity and the left- and right-hand columns show the output near field for focusing and defocusing nonlinearity, respectively. The z coordinate is horizontal in the figures.

where $\Phi(z)=1-\exp(-100z^2/d^2)$ and θ is the step function $\theta(z>0)=1$ and $\theta(z<0)=0$. The electromagnetic field (11) is a wide beam with a Gaussian intensity profile and diameter d having a dark Gaussian notch in the center with five times smaller diameter. The relative phase of the left and right halves of the beam is shifted by 180° so that the field passes through zero at the center and changes sign. The parameters for Fig. 12 are $I_m=3$, $d=100$, and $\epsilon=3\times10^{-2}$. The Gaussian intensity notch in the center of the beam (11) is several times wider than the solitary wave solution (5). This notch [Fig. 12(a)] cannot exist as a whole and after some initial self-focusing [Fig. 12(b)] decays into several narrower dark stripes [Fig. 12(c)] that propagate away from the center of the beam [Figs. 12(d) and 12(e)]. Each of the narrow stripes starts to bend due to the development of the snake instability [Fig. 12(f)] and subsequently breaks up into a set of vortices [Figs. 12(g) and 12(h)]. This breakup is most easily noticeable on several stripes closest to the center of the beam. Figure 13 confirms the existence of the vortices by plotting the real [Fig. 13(a)] and imaginary [Fig. 13(b)] parts of the electromagnetic field and also their product [Fig. 13(c)].

VI. EXPERIMENT: DEFOCUSING CASE

The experimental setup for studying propagation of light beams in a defocusing medium was essentially the same as in the focusing case (see Sec. IV and Ref. [14]). To create a dark stripe parallel to the y axis a glass plate was introduced in half of the beam before the system of two cylindrical lenses. Interference of a reference beam with the light passed through the crystal was used to adjust the tilt of the glass plate to ensure a phase shift of approximately $2\pi n+180°$ between the two halves of the main beam passing through the crystal. The same arrangement was used to visualize zeros of the electromagnetic fields generated as the result of decay of the dark stripe (see [36]). The results below were recorded under steady-state conditions.

Figure 14 shows output intensity profiles of a dark stripe beam for different values of the applied voltage (different values of the nonlinearity) and a fixed level of incoherent illumination. The vertical size of each picture in Fig. 14 is about 200 μm. Figure 14(a) shows the diffractive spreading of the dark stripe embedded in the wider beam and the beam itself for zero applied voltage. As the nonlinearity increases the main beam experiences self-defocusing and the dark stripe starts to self-focus [Fig. 14(b)]. A further increase in the nonlinearity results in the appearance of characteristic snake distortions on the dark stripe due to the transverse modulation instability [Fig. 14(c)]. For still larger nonlinearities the initially continuous dark stripe breaks down into a series of isolated zeros of the electromagnetic field, seen in Figs. 14(d) and 14(e). The existence of the zeros (optical vortices or wave-front dislocations [36]) was confirmed experimentally by interferometric measurements. The spacing of the zeros seen in Fig. 14(e) is about 40 μm, which is in reasonable agreement with the calculated wave numbers of the fastest-growing instability modes of a linearized problem for the solitary-wave solution (5) [14].

We have also shown experimentally that a wider dark stripe decays by the formation of multiple narrower self-focused dark filaments that subsequently start snaking and decay into a series of vortices. An example of such a situation is given in Fig. 15, showing two broken dark stripes embedded in a wide bright beam. The dark stripes have partially decayed into rows of optical vortices.

From the results for both focusing and defocusing nonlinear media it is evident that the asymptotic state of wide

beams propagated through nonlinear media is spatially disordered. Any initially regular structure breaks up into an array of bright or dark filaments. It is thus natural to ask what happens to the spatial statistics when the initial optical field is spatially irregular. To investigate this question we directed a speckle beam through the photorefractive crystal for both focusing and defocusing nonlinearities. As seen on the left-hand side of Fig. 16 for a focusing nonlinearity, regions of the incident beam that were initially relatively bright become brighter, leading eventually to a random array of filaments. In the defocusing case bright regions tend to spread out initially, while for higher nonlinearity we observe multiple dark stripes. In both cases the asymptotic spatial statistics are specific to the sign of the nonlinearity, but independent of the precise realization of the initial conditions.

ACKNOWLEDGMENTS

D.Z.A. and A.A.Z. acknowledge the support of National Science Foundation Grant No. PHY90-12244 and the Optoelectronics Computing Center, an NSF Engineering Research Center. The work at Risø was supported by the Danish Natural Science Research Council.

[1] G. A. Askaryan, Zh. Éksp. Teor. Fiz. **42**, 1567 (1962) [Sov. Phys. JETP **15**, 1088 (1962)].
[2] R.Y. Chiao, E. Garmire, and C.H. Townes, Phys. Rev. Lett. **13**, 479 (1964); **14**, 1056 (1965).
[3] V. E. Zakharov and A. B. Shabat, Zh. Éksp. Teor. Fiz. **61**, 118 (1971) [Sov. Phys. JETP **34**, 62 (1972)].
[4] V. E. Zakharov and A. B. Shabat, Zh. Éksp. Teor. Fiz. **64**, 1627 (1973) [Sov. Phys. JETP **37**, 823 (1973)].
[5] V. E. Zakharov and A. M. Rubenchik, Zh. Éksp. Teor. Fiz. **65**, 997 (1973) [Sov. Phys. JETP **38**, 494 (1974)].
[6] V. I. Bespalov and V. I. Talanov, Pis'ma Zh. Éksp. Teor. Fiz. **3**, 471 (1966) [JETP Lett. **3**, 307 (1966)].
[7] T. B. Benjamin and J. E. Feir, J. Fluid Mech. **27**, 417 (1967).
[8] K. Rypdal and J. Juul Rasmussen, Phys. Scr. **40**, 192 (1989).
[9] N. N. Akhmediev, V. I. Korneev, and R. F. Nabiev, Opt. Lett. **17**, 393 (1992).
[10] E. A. Kuznetsov and S. K. Turitsyn, Zh. Éksp. Teor. Fiz. **94**, 119 (1988) [Sov. Phys. JETP **67**, 1583 (1988)].
[11] G. S. McDonald, K. S. Syed, and W. J. Firth, Opt. Commun. **95**, 281 (1993).
[12] C. T. Law and G. A. Swartzlander, Jr., Opt. Lett. **18**, 586 (1993).
[13] A. V. Mamaev, M. Saffman, and A. A. Zozulya, Europhys. Lett. (to be published).
[14] A. V. Mamaev, M. Saffman, and A. A. Zozulya, Phys. Rev. Lett. **76**, 2262 (1996).
[15] V. Tikhonenko, J. Christou, B. Luther-Davies, and Y. S. Kivshar (unpublished).
[16] H. Jerominek, R. Tremblay, and C. Delisle, J. Lightwave Technol. **LT-3**, 1105 (1985); H. Jerominek, C. Delisle, and R. Tremblay, Appl. Opt. **25**, 732 (1986).
[17] For a review of self-focusing of large circular beams see, e.g., Y. R. Shen, *The Principles of Nonlinear Optics* (Wiley, New York, 1984).
[18] M. D. Iturbe-Castillo *et al.*, Appl. Phys. Lett. **64**, 484 (1994).
[19] M. D. Iturbe-Castillo *et al.*, Opt. Commun. **118**, 515 (1995).
[20] G. Duree *et al.*, Phys. Rev. Lett. **71**, 533 (1993); M.-F. Shih *et al.*, Electron. Lett. **31**, 826 (1995).
[21] G. Duree *et al.*, Phys. Rev. Lett. **74**, 1978 (1995); M. Taya *et al.*, Phys. Rev. A **52**, 3095 (1995).
[22] A. A. Zozulya and D. Z. Anderson, Phys. Rev. A **51**, 1520 (1995).
[23] A. A. Zozulya and D. Z. Anderson, Opt. Lett. **20**, 837 (1995).
[24] V. V. Voronov, I. R. Dorosh, Yu. S. Kuz'minov, and N. V. Tkachenko, Kvant. Elektron. **7**, 2313 (1980) [Sov. J. Quantum Electron. **10**, 1346 (1980)].
[25] J. Feinberg, J. Opt. Soc. Am. **72**, 46 (1982).
[26] A. A. Esayan, A. A. Zozulya, and V. T. Tikhonchuk, Sov. Phys. Lebedev Inst. Rep. **5**, 45 (1990).
[27] A. A. Zozulya, M. Saffman, and D. Z. Anderson, Phys. Rev. Lett. **73**, 818 (1994).
[28] S. Gatz and J. Herrmann, J. Opt. Soc. Am. B **8**, 2296 (1991).
[29] G. C. Valley *et al.*, Phys. Rev. A **50**, R4457 (1994); M. Segev *et al.*, Phys. Rev. Lett. **73**, 3211 (1994).
[30] A. A. Zozulya and D. Z. Anderson (unpublished).
[31] M. J. Ablowitz and H. Segur, *Solitons and the Inverse Scattering Transform* (SIAM, Philadelphia, 1981); V. E. Zakharov, S. V. Manakov, S. P. Novikov, and L. P. Pitaevsky, *Theory of Solitons* (Consultants Bureau, New York, 1984).
[32] A. Barthelemy, S. Maneuf, and C. Froehly, Opt. Commun. **55**, 201 (1985); M. Shalaby and A. Barthelemy, Opt. Lett. **16**, 1472 (1991).
[33] M. D. Iturbe-Castillo *et al.*, Opt. Lett. **20**, 1853 (1995).
[34] G. R. Allan *et al.*, Opt. Lett. **16**, 156 (1991); G. A. Swartzlander, Jr. *et al.*, Phys. Rev. Lett. **66**, 1583 (1991); G. A. Swartzlander, Jr. and C. T. Law, *ibid.* **69**, 2503 (1992); B. Luther-Davies, R. Powles, and V. Tikhonenko, Opt. Lett. **19**, 1816 (1994).
[35] Yu S. Kivshar, IEEE J. Quantum Electron. **28**, 250 (1993).
[36] N. B. Baranova *et al.*, Pis'ma Zh. Éksp. Teor. Fiz. **33**, 206 (1981) [JETP Lett. **33**, 195 (1981)]; B. Ya. Zel'dovich, A. V. Mamaev, and V. V. Shkunov, *Speckle-Wave Interactions in Application to Holography and Nonlinear Optics* (CRC, Boca Raton, FL, 1995).